Available online at www.sciencedirect.com

SCIENCE DIRECT®

Nuclear Instruments and Methods in Physics Research A 498 (2003) 292–311

NUCLEAR INSTRUMENTS & METHODS IN PHYSICS RESEARCH Section A

www.elsevier.com/locate/nima

Performance of the 10 m^3 ICARUS liquid argon prototype

F. Arneodo[a], A. Badertscher[b], B. Baiboussinov[c], G. Battistoni[d], P. Benetti[e], E. Bernardini[a], M. Bischofberger[b], A. Borio di Tigliole[e], R. Brunetti[e], A. Bueno[b], E. Calligarich[e], M. Campanelli[b], C. Carpanese[b], D. Cavalli[d], F. Cavanna[f], P. Cennini[g], S. Centro[c], A. Cesana[h], C. Chen[i], D. Chen[i], Y. Chen[i], D. Cline[j], C. De Vecchi[e], A. Di Credico[a], R. Dolfini[e], A. Ferrari[g,d], F. Ferri[a], A. Gigli Berzolari[e], I. Gil-Botella[b], L. Grandi[e], A. Grillo[a], A. Haag[f], K. He[i], X. Huang[i], A. Kruse[b], M. Laffranchi[b], Z. Li[i], M. Lisowski[b], F. Lu[i], J. Ma[i], C. Matthey[j], F. Mauri[e], D. Mazza[f], G. Meng[c], C. Montanari[e], S. Muraro[d], S. Navas-Concha[b], M. Nicoletto[c], G. Nurzia[f], S. Otwinowski[j], Q. Ouyang[i], O. Palamara[a,*], D. Pascoli[c], L. Periale[k,l], S. Petrera[f], G. Piano Mortari[f], A. Piazzoli[e], P. Picchi[l,m,k], F. Pietropaolo[c], T. Rancati[d], A. Rappoldi[e], G.L. Raselli[e], J. Rico[b], B. Romualdi[a], M. Rossella[e], A. Rotilio[a], A. Rubbia[b], C. Rubbia[e], P. Sala[d], D. Scannicchio[e], E. Scapparone[a], E. Segreto[f], F. Sergiampietri[n], N. Sinanis[b], E. Tatananni[a], M. Terrani[h], S. Ventura[c], C. Vignoli[e], H. Wang[j], J. Woo[j], G. Xu[i], Z. Xu[i], C. Zhang[i], Q. Zhang[i], S. Zhen[i]

[a] *INFN - Laboratori Nazionali del Gran Sasso, s.s. 17bis Km 18+910, Assergi, L'Aquila, Italy*
[b] *Institute for Particle Physics, ETH Hönggerberg, Zürich, Switzerland*
[c] *Dipartimento di Fisica e INFN, Università di Padova, via Marzolo 8, Padova, Italy*
[d] *Dipartimento di Fisica e INFN, Università di Milano, via Celoria 16, Milano, Italy*
[e] *Dipartimento di Fisica e INFN, Università di Pavia, via Bassi 6, Pavia, Italy*
[f] *Dipartimento di Fisica e INFN, Università dell'Aquila, via Vetoio, L'Aquila, Italy*
[g] *CERN, CH-1211 Geneva 23, Switzerland*
[h] *Politecnico di Milano (CESNEF), Università di Milano, via Ponzio 34/3, Milano, Italy*
[i] *IHEP—Academia Sinica, 19 Yuquan Road, Beijing, People's Republic of China*
[j] *Department of Physics, UCLA, Los Angeles, CA 90024, USA*
[k] *IFSI—Torino, corso Fiume 4, Torino, Italy*
[l] *Dipartimento di Fisica, Università di Torino, Via Giuria 1, Torino, Italy*
[m] *INFN—Laboratori Nazionali di Frascati, Via E. Fermi 40, Frascati, Rome, Italy*
[n] *INFN—Pisa, via Livornese 1291, San Piero a Grado, Pisa, Italy*

Received 4 November 2002; accepted 11 November 2002

---

*Corresponding author. Tel.: +39-0862-437553; fax: +39-0862-437570.
E-mail addresses: ornella.palamara@lngs.infn.it (O. Palamara).

0168-9002/03/$ - see front matter
doi:10.1016/S0168-9002(02)01989-7

Abstract

We report on the performance of a liquid Argon Time Projection Chamber, operating in a 10 m^3 cryostat. This device built in the framework of the ICARUS T600 programme to serve as a full test facility for the adopted cryogenics and mechanical solutions, was successfully tested in 2000 as the last step before the tests of the first 600 t ICARUS module 1 year later. In a final run at the Gran Sasso Laboratory, whose outcome provides the main subject of this paper, also the readout and imaging capabilities of the installed wire chamber and the overall performance of the detector have been successfully tested.

PACS: 29.40.Gx; 29.40Vj; 29.85 + c; 29.90 + r

Keywords: Liquid argon; TPC; Track reconstruction

1. Introduction

ICARUS is a project for the construction of a large mass Liquid Argon Time Projection Chamber (LAr TPC) to be installed in the Gran Sasso Underground Laboratory (LNGS, Italy) for the study of neutrino physics from various sources (atmospheric, solar, Supernova and artificial long-baseline ν beam) and for rare events detection, such as nucleon decay. Many years of R&D have allowed to overcome the technological difficulties in the realization of the ICARUS *bubble chamber*-like technique. The ICARUS LAr TPC technique is now mature: the most recent successful operation of the first 600 t ICARUS module ("T600") [1,2] in Pavia has ultimately opened the way for experimental applications.

An important step in the ICARUS project has been the transfer of the R&D outcome to industry. This is the only way to go from laboratory scale detectors to the large masses required by the physics goals aimed at. A major breakthrough came with the realization of a large prototype (14 t of LAr, usually indicated as the "10 m^3 module", the LAr density being 1.4 g/cm^3) built in 1997 by Air Liquide cryogenics company. The 10 m^3 was originally conceived as a prototype to test all the technical solutions adopted for the design of the T600 module. In fact, the 10 m^3 module is exactly a "slice" of one half-module of the T600 detector. The cooling system, the LAr purification systems are a one-to-one copy of the corresponding features in use in the T600 module. The wire chamber placed inside also reproduces the geometry and the mechanics of the T600 TPC, excepting the dimensions, in order to fit the reduced volume of the 10 m^3 module, and the number of wire planes, limited to two instead of three planes as in the T600 TPC. Finally, as in the T600 case, the inner detector layout of the 10 m^3 includes photomultipliers (PMTs) for a prompt detection of the light emitted in LAr at the passage of ionizing particles.

The cryogenics and the Ar purification systems as well as the performance of the mechanics of the inner detector have been extensively tested in Pavia, where several cooling and filling tests successfully ended in July 1999 [3].

A second test phase (the main subject of the present paper) occurred from January to June 2000 at LNGS. The goal was the study of the detector performance by exposing it to surface cosmic rays. Moreover, the technical solutions adopted for the final ICARUS design (from cryogenics to data acquisition system) and the overall detector stability were explored in a ($\sim$100 days) long-term operation.

The sample of collected events includes a variety of different cosmic ray topologies, such as single muons crossing the LAr volume, muon bundles and showering events with electro-magnetic and/or hadronic components. On the basis of this data sample we have developed and optimized the off-line event reconstruction and analysis algorithms to study the performance of the 10 m^3 detector.

The main issues of the analysis reported here are: optimization of the signal extraction procedures, measurements of the electron drift velocity and of the electron life-time in LAr, calorimetric reconstruction of the events [4]. A paper on the study of light collection from the PMTs immersed in LAr is in preparation.

2. The ICARUS technology

The main aim of the ICARUS technique [5] is to detect the ionization charge released at the passage of charged particles in a volume of LAr with three-dimensional image reconstruction and calorimetric measurements of the ionizing events. A uniform electric field is applied to the medium; thanks to the low transverse diffusion of the ionization charge the electron images of ionization tracks are preserved and projected onto the anode, following the electric field lines. The read-out of the electron image at the anode can be realized by implementing a system of successive wire planes biased at different potentials so that simultaneous and independent measurements of the drifting charge can be accomplished (*non-destructive* read-out). Measurements of the electron drift time at several points along the track provide the track coordinates on a direction parallel to the electric field lines. The wires are oriented on each plane at a different angle and therefore a three-dimensional image can be reconstructed from the combination of the wire coordinate on each plane at a given drift time. Measurement of the so-called "T_0 time" (associated to the passage of the particle through the active medium) combined with the drift velocity information provides the absolute position of the tracks along the drift coordinate. Determination of T_0 can be accomplished by prompt detection of the scintillation light produced by ionizing particles in LAr [6]. For this purpose suitable PMT arrays are implemented inside the LAr volume.

3. The 10 m^3 module

The 10 m^3 detector was designed to reproduce as close as possible the working conditions of the final T600 module. The LAr container is a parallelepiped, vacuum tight box, $2.58w \times 3.98h \times 1.00l$ m^3 (internal dimensions), made of 150 mm thick aluminium honeycomb panels. The container is externally equipped with a cryogenics system, to keep the liquid Argon volume at stable temperature, and with a suitable purification system. The sensitive detectors (TPC and PMTs) are mounted inside the container. The main geometrical characteristics of the 10 m^3 module are summarized in Table 1.

Table 1
Geometrical characteristics of the 10 m^3 module

Container internal dimensions	
Width	2.58 m
Height	3.98 m
Length	1.00 m
Container material (honeycomb structure)	Aluminium
Wall thickness	150 mm
External insulation thickness	465 mm
Total LAr volume	10.0 m^3
Total LAr mass	13.9 t

3.1. The cryogenics system

A schematic view of the module cryogenics plant for Ar cooling and purification is shown in Fig. 1. Cooling of LAr is provided by a forced circulation of pressurized liquid nitrogen (LN_2) inside a circuit directly inserted into the aluminium panels. The container is surrounded by an insulation layer (465 mm thick) made of aramid fiber honeycomb panels (see Table 1). The system is designed so that the temperature of the LAr is kept uniform within one degree. This is to avoid relevant variations of the electron drift velocity over the internal volume. The top cover panel is removable to allow for the insertion of the internal detector (wire chamber module, sensors and monitors). The signal feed-through's of the wire chamber and of the sensors, the entry points of the

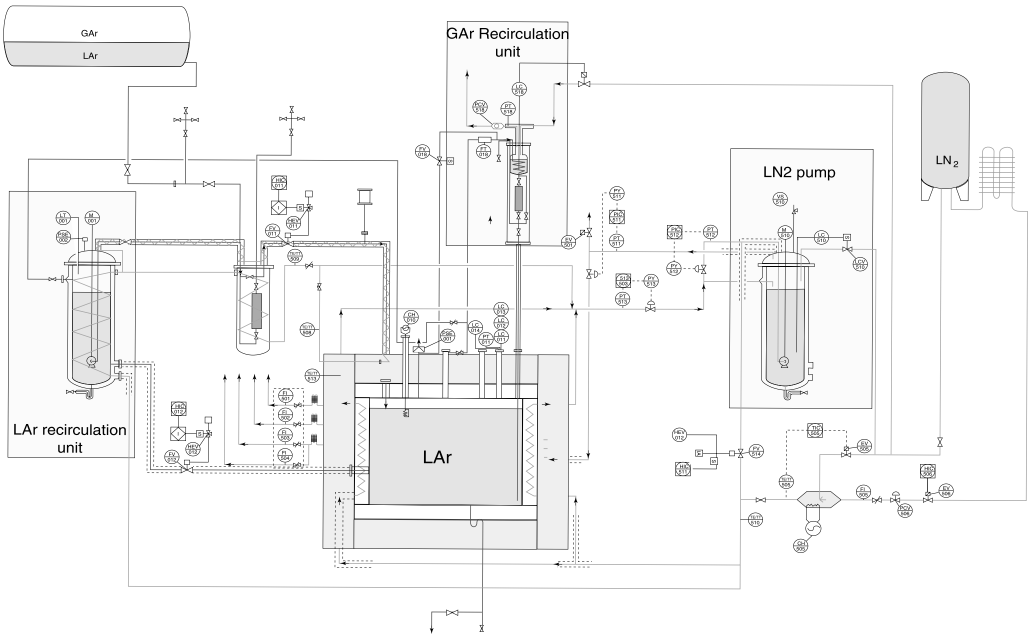

Fig. 1. Schematic layout of the 10 m^3 cryogenics plant. The Ar purification and re-circulation units for the liquid and gas phase, as well as the LN_2 pump of the cooling system are visible, with their connections to the LAr cryostat.

main purification and the re-circulation systems are located on the top cover.

The module is equipped with:

(1) a liquid phase re-circulation unit composed by a oxisorb/hydrosorb standard filter housed in an ancillary cryostat and with a cryogenics pump, also housed in an external cryostat, used to force LAr circulation through the filter.
(2) a argon gas (GAr) re-circulation unit containing a oxisorb/hydrosorb standard filter.

The LAr re-circulation system has the advantage that the phase does not need to be changed. Thus, the re-circulated Ar flow is almost three orders of magnitude (the ratio of densities) higher than through the GAr unit. The GAr re-circulation system is necessary to directly clean the Ar gas above its free surface, where we expect impurities to be produced by material outgassing from the warm parts of the detector (roof of the cryostat, cables, flanges, electrodes, etc.).

The 10 m^3 module is also equipped with an automatic control and regulation system of the cryogenics plant, a simplified version of the one designed for the T600 module. It automatically regulates the various processes during the run (cooling process, pumps functionality, automatic valves opening and regulation, filling of dewars, etc.). The system is controlled by a PC and its interface provides a schematic display of the plant conditions (pressures, temperatures, etc.) and activates alarms in case of malfunctioning. Several types of sensors have been added inside the cryostat to complete the equipment of the module, namely LAr level meters, temperature and pressure probes and LAr purity monitors [7].

3.2. The wire chamber

The TPC and its mechanical structure is housed inside the cryostat volume and consists of a stainless steel frame for two vertical, coplanar wire planes placed at 3 mm from each other. The total number of wires is 1856 (928 per plane). The

Fig. 2. The mechanical structure holding the wire planes in its initial configuration for the Pavia test, before insertion in the $10\ m^3$ container. The springs acting on the weight-bridge, elements of the "variable geometry" layout, are visible at the bottom of the front side of the structure.

wires are made of stainless steel with a wire diameter of 150 μm. The wire pitch is 3 mm. Wire directions in the two planes run, respectively, at $+60^\circ$ and -60° from the horizontal. The length of the wires varies from 0.4 to 3.8 m. The wires are anchored in groups of 32 units to special holders embedding a printed board. Each printed board can be connected to a twisted pair flat cable for the signal transfer outside the cryostat via specially designed vacuum-tight feed-through flanges. A set of calibrated springs attached on the backside of the rocking frames that hold the wires (weight-bridge) compensates for the tension increase on the wires, preventing the risk of wire breaking due to over-stress during the cooling phase ("variable geometry" concept). The overall dimensions of the mechanical structure holding the wire planes are $2.13w \times 3.93h\ m^2 \times 0.91l$ m and the weight is about 2 t (see Fig. 2). The main parameters of the wire chamber are summarized in Table 2.

Table 2
Main parameters of the $10\ m^3$ module internal detector

Number of wire planes	2
Distance between wire planes	3.0 mm
Number of wires / plane	928
Total	1856
Wire diameter (stainless steel)	150 μm
Wire length	0.40–3.82 m
Wire pitch	3.0 mm
Wire orientation with respect to horizontal	$\pm 60^\circ$
Cathode plane	stainless steel
Width	2.00 m
Height	3.26 m
Distance to wire planes	0.35 m
Number of *race-tracks* rectangular rings	6
Ring width	1.95 m
Ring height	3.21 m
Ring tube (stainless steel) diameter	3.5 cm
Distance between *race-tracks* rings	5.0 cm
Maximum drift length	0.35 m
Maximum drift time	
at 285 V/cm	0.30 ms
at 500 V/cm	0.22 ms
Sensitive volume dimensions	
Width	2.00 m
Height	3.26 m
Length	0.35 m
Total sensitive volume	$2.28\ m^3$
Total sensitive LAr mass	3.2 t

4. The Pavia run

The cryogenics and purification systems of the $10\ m^3$ module have been tested at the Pavia INFN site. The test programme aimed at the acquisition of data for the determination of the main features of the cryogenics and purification systems: vacuum tightness, cool-down slope, temperature gradients, purification and re-circulation systems performance. The operation of the $10\ m^3$ during the Pavia run has been a milestone in the ICARUS R&D activity in order to test the reliability of the "variable geometry" solution for the wire tensioning and the influence of the employed materials on the LAr purity level.

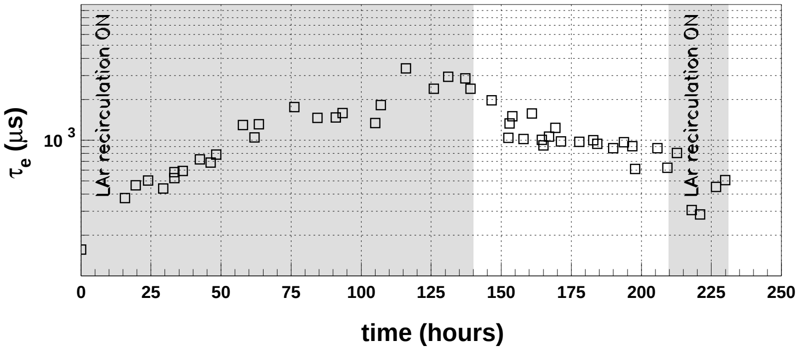

Fig. 3. Evolution of the electron life-time in LAr measured using the purity monitors (Pavia run). The shaded zone indicates the period with the LAr forced re-circulation on.

A start-up procedure of the cryogenic plant has been identified and tested. It consists of four steps: vacuum pumping in the LAr container and test of its mechanical behaviour, pre-cooling of the LAr container with Nitrogen gas, cooling with LN_2 and filling of the container with LAr. The overall operation takes about 15 days. The residual vacuum after pumping was at the level of $\sim 5 \times 10^{-6}$ mbar. The pre-cooling and the cooling systems worked efficiently: at the end of the pre-cooling phase a temperature of about 220 K was uniformly achieved inside the detector. Then, cooling with LN_2 was started. The temperature of the walls of the LAr container and of the wire chamber structure dropped regularly down to the LAr temperature (87 K). The system suffered no instability during the whole procedure. The LAr filling phase then started. Completion of the LAr filling took about 35 h.

The initial value of the electron life-time (τ_e) measured with the LAr purity monitors just after the filling of the cryostat with LAr was in the 100 µs range. The LAr pump of the liquid phase purification system was then turned on to enhance the level of LAr purity: after 4 days of forced re-circulation of the liquid through the purifier, the drift electron life-time extended beyond 2 ms (see Fig. 3). The level of purity achieved in the 10 m^3 shows that the technique is mastered at a level at which very long drift distances are conceivable. This is an important feature for the scaling to very large LAr volumes.

After stopping the LAr pump and without operating the GAr re-circulation unit, a slow purity degradation is expected due to residual internal out-gassing. We observed indeed this behaviour as shown in Fig. 3.

At the end of the test the wire chamber was extracted. None of the wires got broken and the chamber structure did not suffer evident deformations, demonstrating the reliability of the wire tensioning scheme based on the "variable geometry" concept.

5. The LNGS run

The successful operation of the 10 m^3 during the test run in Pavia concluded the R&D phase concerning the cryogenics, purification and internal detector mechanics in view of the T600 realization. The 10 m^3 module was then dismounted and transported to the LNGS external facility *Hall di Montaggio* for a further test run [8]. This phase aimed at a full test of the 10 m^3 as a detector module, i.e. at the collection of ionizing events with the wire chamber. To achieve this goal the read-out electronics and DAQ system had to be implemented and a number of essential components had to be added to the inner detector.

5.1. Inner detector

The layout of the inner detector was completed according to the ICARUS T600 design by adding:

- A cathode, to establish a uniform electric field across the LAr volume. It consists of a thin

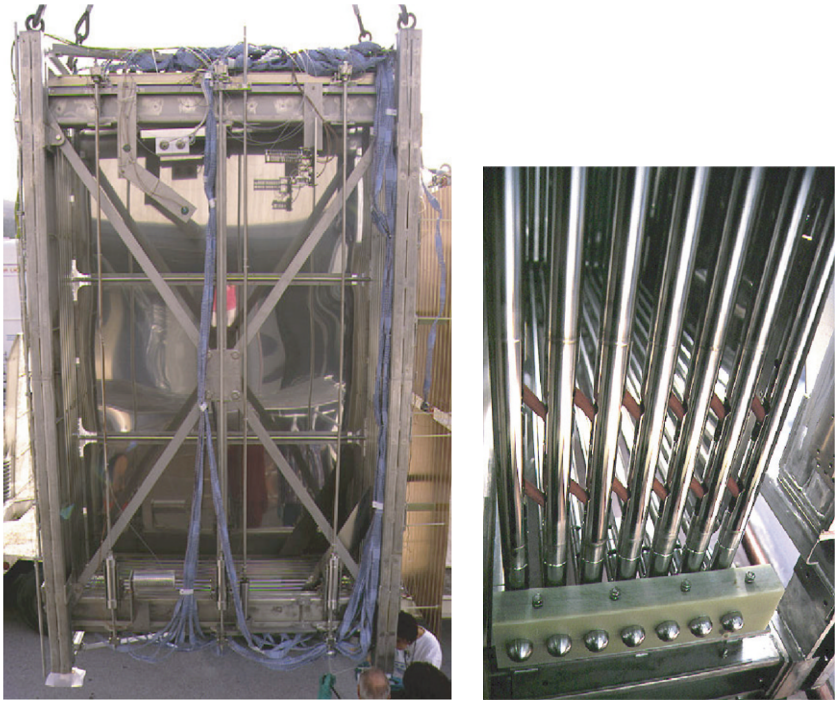

Fig. 4. (Left) The mechanical structure of the inner detector in its final configuration for the LNGS test, before the insertion into the cryostat (front view). The reflecting surface is the cathode. Also visible are the signal cables connected to the wires, the PMTs (upper left), and the LAr purity monitors (upper right). (Right) Side view of the mechanical structure: Detail of the race-tracks.

stainless steel plane with surface dimension equivalent to the wire planes (Fig. 4 (left) and Table 2). The cathode is parallel to the wire plane and placed 35 cm apart. This distance corresponds to the maximum drift length allowed by the internal dimensions of the cryostat.

- A High Voltage (HV) feed-through with a dedicated electrical contact to the cathode.
- A field shaping system (*race-tracks*, see Fig. 4 (right) and Table 2), which allows to keep a high electric field uniformity even at the drift volume boundaries. The field shaping system was realized and assembled according to the T600 design. It consists of six rectangular co-axial rings ($1.95w \times 3.21h$ m^2) made of stainless steel cylindrical tubes (3.5 cm of diameter). The rings are positioned in planes perpendicular to the electric field direction (the drift axis) at 5 cm from each other. The *race-tracks* system is electrically connected to the cathode HV power supply with each ring set at the appropriate voltage by means of a resistor chain. To this purpose each ring embeds a socket for the insertion of 50 MΩ special resistors for cryogenics applications. The last ring nearest to the wire plane is grounded.
- Printed boards embedded in the wire holders, for the connection to the wire-end pins, and twisted pair cables, for the connection between the printed boards and the external feed-through's. The cable capacitance per unit of length is about 40 pF/m. The length of the cables is 4 m (8 m) for the connection of the printed boards located on the upper (lower) beam of the wire chamber frame.
- A PMT system for light detection. Two 2″ PMTs have been installed behind the wire planes, facing the drift volume. The optical window of one of them has been covered with Sodium Salicilate as wavelength shifter to extend the sensitivity down to the wavelength

Fig. 5. The 10 m^3 set-up during the run at the LNGS. The GAr re-circulation unit and a rack with the read-out electronics are visible on the top, as well as the external trigger scintillators on two opposite sides and the LN_2 pump on the right. The LAr purification circuit is behind, hidden by the cryostat.

of scintillation light in LAr (128 nm)[1] [6]. The PMT system may provide prompt internal trigger signals also useful for T_0 measurement.

An additional external trigger system based on plastic scintillator slabs has been mounted on two opposite external walls of the cryostat (see Fig. 5) to provide suitable trigger for events with a definite geometry. The triggered events give, in this case, long track muons which traverse the drift volume almost parallel to the wire planes, inducing quasi-simultaneous signals on a large fraction of the wires.

The upgrade resulted in a fully instrumented TPC (see Table 2 for the list of main parameters) with two wire coordinates plus drift time with a sensitive volume of $(2.00w \times 3.26h \times 0.35l)$ m^3. In the following we call *induction* wire plane the one nearest to the cathode (i.e. the first along the drift direction, reading the charge induced by the drifting electrons) and *collection* wire plane the other one (working in charge collection mode).

In Fig. 4 (left) the internal detector just before the insertion into the cryostat is shown. Mounting of the cryogenic plant (passive insulation panels, LAr and LN_2 circuits) completed the detector set-up. The 10 m^3 prototype during the test at the external LNGS facility is shown in Fig. 5.

[1] In the T600 module the PMTs are of different type and dimensions (8″ window) and the wavelength shifter is also different (TPB, Tetra-Phenyl-Butadiene).

5.2. Electronics and DAQ

The readout electronics implemented for the LNGS run follows the T600 design. It is structured as a multi-channel waveform recorder that continuously stores charge information collected by each wire during the drift of the electrons. The read-out chain is composed of:

- A "decoupling board" that receives analog signals from the TPC wires through vacuum tight feed-through flanges and passes them to the "analog board" after decoupling the wire signal from the electrical bias. This board is housed in the back-plane of a VME crate ("the analog crate"). It also provides the biasing of the wires and the distribution of calibration signals.
- A VME (CAEN V791) module, the "analog board" [9], where the wire signal is shaped and amplified, and subsequently sampled by a 10 bit flash ADC. There are two ADCs per board, clocked at 40 MHz, each one serving 16 multiplexed channels. The single wire sampling frequency is therefore 2.5 MHz. The analog boards (up to 18 units) are housed in a single analog crate.

  The V791 boards come in two versions with different shaping time constants: the "Q" ("C") version adopts a shaping time of ~ 50 μs (~ 3 μs). "C" type boards have been adopted for the *induction* plane and "Q" boards for the *collection* plane. The recorded signal shapes from the two planes are different, due to the different shaping time of the boards as well as to the different kind of signals detected by the wires of the two planes. This requires the use of different algorithms at off-line level for the analysis of the signals from the two planes, as explained in Section 6.

- A digital board (VME CAEN V789) [10] where the digitized waveforms are transferred from the analog board via an external cable. It features a circular memory buffer, whose depth can be tuned to the detector drift length. In the 10 m^3 case, 1024 time samples (each one corresponding to 0.4 μs) have been used to encompass the 35 cm maximum drift (at a typical value of 300 V/cm of the electric field the drift velocity is 1.2 mm/μs). Each digital board serves 32 wire-channels. A VME crate, "the digital crate", hosts up to 18 V789 boards.

Each digital crate hosts a CPU (Motorola VME 2100 with VxWorks operating system) that manages the transfer of the data to an Event Manager process (running on a Sun workstation), via an Ethernet link. Once a trigger is issued each V789 board in the digital crate is queried for the buffered data. The data packets coming from each CPU are then put together by the Event Manager process for event display and disk storage.

5.3. Data taking

Operation with the complete set-up at LNGS was started with the same start-up procedure used during the Pavia test (Section 4). The run period lasted about 100 days. The first part of this period was dedicated to LAr purification and relative life-time measurements and to the implementation and test of the read-out electronics and DAQ.

The evolution of the electron life-time at different conditions of the liquid phase purification system has been recorded with the purity monitors. Without operating the GAr re-circulation unit, a purity degradation after stopping the LAr pump was observed (Fig. 6). This cycle was repeated several times during the run.

Up to 960 electronics channels have been progressively instrumented, 480 channels on each of the two wire planes, providing two views of ionizing events. The instrumented wires corresponded to the sector of the wire chamber facing the LAr volume seen by the internal PMTs (see Fig. 4 (left)).

A dedicated test of noise induced by the cryogenics and purification systems to the wire signals was performed. No significant variation on the signal spectrum from the read-out wires was observed by turning on and off the various devices of the cryogenic system (vacuum pumps, LN_2 pump, LAr pump). This indicates that the noise induced by the cryogenics system is negligible.

Ionizing events with the maximum available number of instrumented read-out wires were recorded in the last 30 days of the data taking period. In total, about 12,000 cosmic-ray triggers (including technical runs) have been collected using both the PMTs and the external systems.

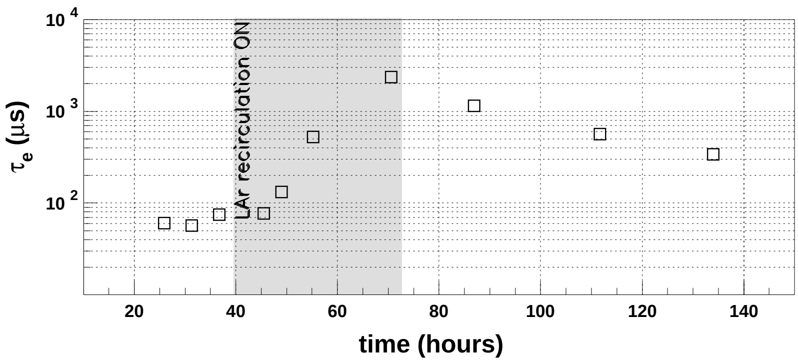

Fig. 6. Evolution of the electron life-time in LAr measured using the purity monitors, during the first few days after start-up (LNGS run). The shaded zone indicates the period with the LAr forced re-circulation on.

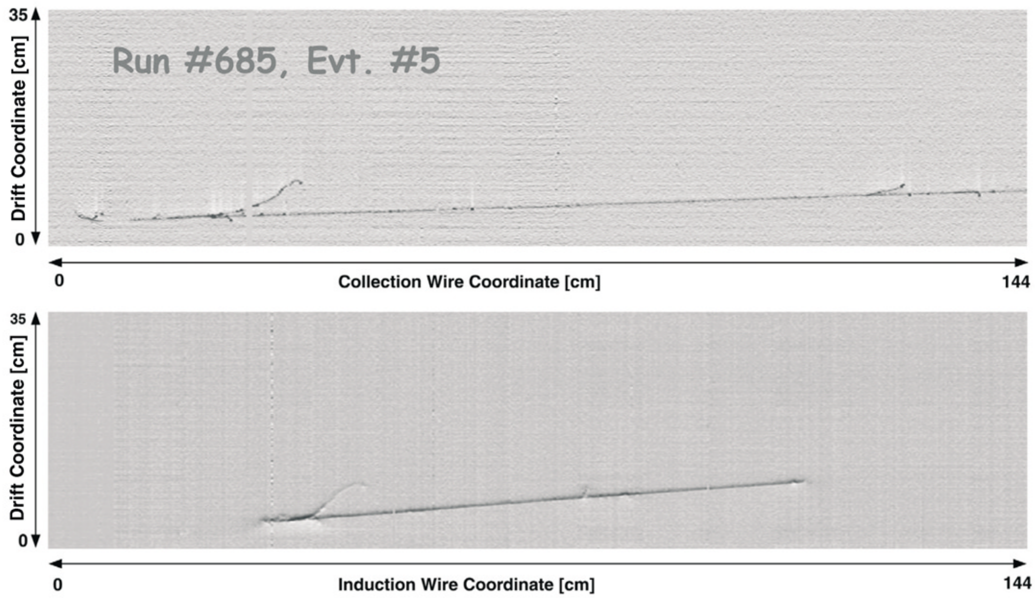

Fig. 7. Induction and collection 2D views of a typical cosmic muon crossing the LAr sensitive volume. δ-rays well separated along the main track are also visible. The trigger was provided by the external scintillator counters.

The value of the electric field in the drift region was varied during operation from 285 to 500 V/cm. Voltage bias on the *induction* and *collection* wire planes was also correspondingly varied. The technical runs were analyzed for the tuning of the electric fields in the active volume and between the wire planes. This allowed to optimize the transparency of the *induction* wire plane to the drifting electrons.

The images of the events collected after optimization of the HV parameters prove the capability to provide fine grain spatial resolution allowing very good multiple tracks separation. A variety of different cosmic-ray signatures has been recorded: from tracks of single muons crossing the active volume or stopping and decaying into electron to more complicated multi-track topologies with muon bundles, electromagnetic and hadronic showers. Single track events have been selected for the off-line analysis reported in this paper. An example of events recorded in the *collection* and *induction* views is shown in Figs. 7 and 8. In these pictures, for each of the wires (horizontal coordinate) the recorded signal is displayed as a function of the drift time (vertical coordinate). The level of gray of the pixel codes the signal pulse height. This provides a 2D image of the ionization track projected on each wire plane.

6. Signal processing and event reconstruction

Underlying the images, such as in Figs. 7 and 8, there are the recorded waveforms of each wire. This is more clearly shown in Fig. 9 (left) where the raw waveforms for a number of adjacent wires of the *induction* plane are displayed. The full advantage of the ICARUS technology is exploited through an accurate signal waveform processing.

For this purpose, a detailed study of the recorded waveforms (amplitude measured as a function of the drift time on individual wires) has been performed aiming at the optimization of the different stages of the signal processing [10,11]. The first step consists of a filtering procedure to reduce possible noise components.

Physical signals are characterized by distinctive shapes in the *collection* and *induction* view waveforms (see Section 5.2). *Collection* signals manifest a step-like shape followed by the exponential

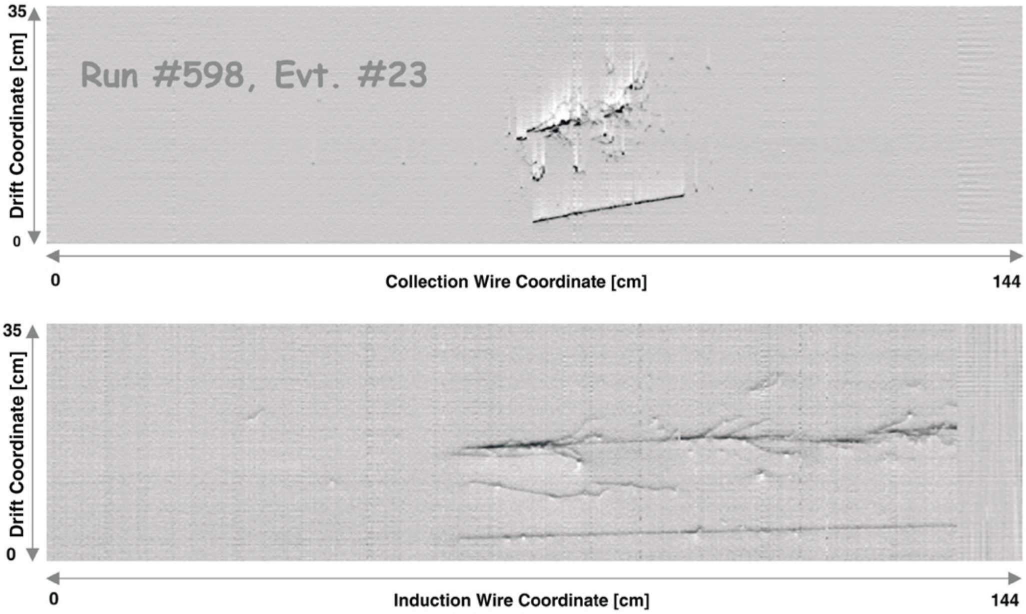

Fig. 8. Induction and collection 2D views of an event with a muon track and a low energy electro-magnetic shower. The trigger was provided by the internal PMTs.

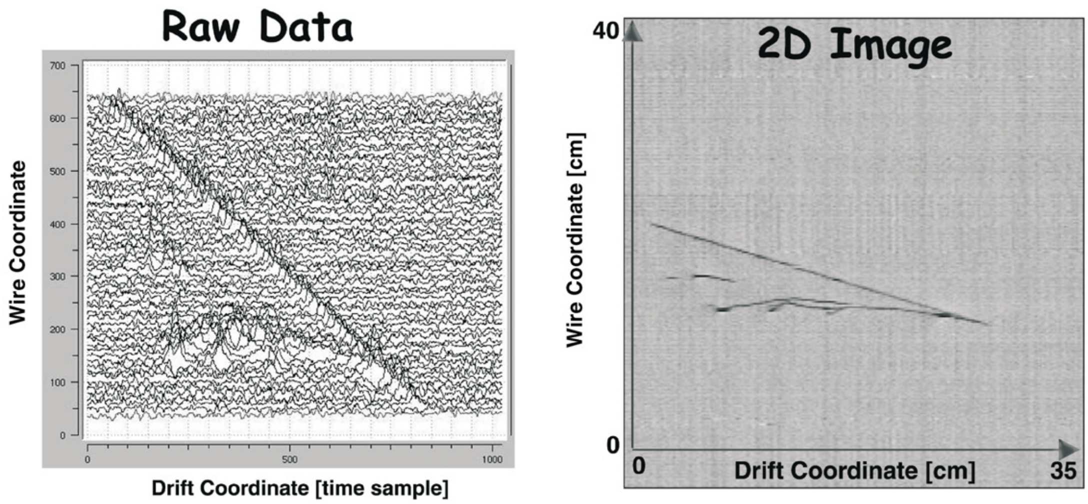

Fig. 9. (left) Display of digitised waveforms recorded from a number of induction wires detecting an event and (right) the event image after gray-level coding of the waveform pulse-height.

discharge of the amplifier (see Fig. 10); *induction* signals, instead, show bipolar shapes with quite narrow peaks (see Fig. 11 (right)). However, the relative amplitude of the peaks and the signal shape may vary due to the orientation of the track in the sensitive volume, to the distance of the track from the wire plane and to the ionization density [12]. In many cases the first (negative) peak is

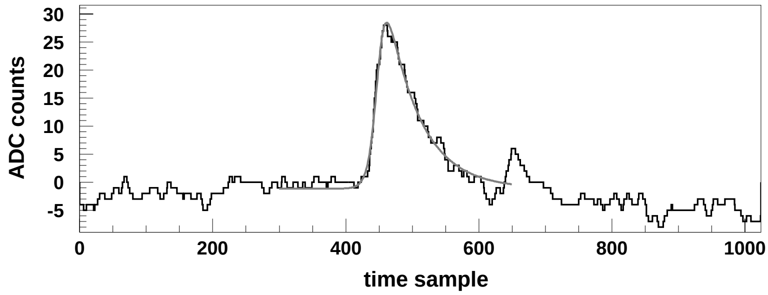

Fig. 10. Digitised waveform from a wire of the collection plane. A time sample corresponds to 0.4 μs. The peak above the baseline is due to the charge collection of the portion of a single muon track "seen" by the wire. The continuous line shows the result of the fit with the $F_c(t)$ function of Eq. (1) in a time window around the Region of Interest (ROI).

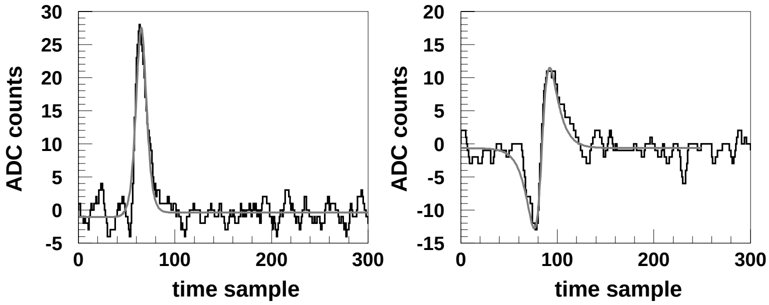

Fig. 11. (left) Unipolar and (right) bipolar digitized waveforms from the induction wire plane in a time window around the ROI. The time sample is 0.4 μs. The continuous lines show the results of the fit with the $F_i(t)$ function of Eq. (2).

reduced and hidden by the baseline fluctuations and the signal assumes a unipolar-like shape (see Fig. 11 (left)).

Searching for rising edges and proper shapes of the waveforms one can identify Regions of Interest (ROIs, i.e. regions containing the signal peak above the baseline). Using suitable algorithms we extract the physical parameters of the signal inside the ROI, and define a "hit" by (1) the signal amplitude proportional to the deposited charge, (2) the peak time that gives the drift coordinate and (3) the rise time. For *collection* wires the signal amplitude is given by the amplitude of the peak. For *induction* wires it is given by the integration of the signal above the baseline.

The extraction of the physical parameters from the waveforms can be further optimized by using analytical functions for their fit. The analytical expressions chosen are quite flexible and able to reproduce different data by means of a few parameters. Different fitting functions have been developed for the two views. The analytical expression giving the best results in fitting the *collection* waveforms is the following function of the drift time (t):

$$F_c(t) = A_c \frac{e^{(t_0-t)/\tau}}{1+e^{(t_0-t)/R_t}} + B_c \tag{1}$$

where t_0 is the signal peak time, τ is the signal decay time (depending on the amplifier decay constant), R_t is the signal rise-time (depending on the inclination of the track), B_c is the baseline amplitude and A_c is a normalization factor (depending on the peak pulse height). An example is given in Fig. 10, it shows a recorded waveform with the fitted curve superimposed to it.

The function developed to fit the *induction* waveforms, which has the peculiarity of describing both unipolar and bipolar shapes, is

$$F_i(t) = A_i \frac{e^{-(t_0-t)/R_2}}{1+e^{-(t_0-t)/R_1}} \times \left[\frac{e^{-(t_0-t)/R_1}/1+e^{-(t_0-t)/R_1}}{R_1} - \frac{1}{R_2}\right] + B_i \tag{2}$$

where t_0 is the point of inflection of the function, R_1 is the positive amplitude signal rise-time, R_2 is the negative amplitude signal rise-time, B_i is the baseline amplitude and A_i is a normalization factor. Examples of the results of the fit are given in Fig. 11.

After waveform processing, two 2D views are obtained for each event by combining the informations from drift time and amplitude of the hits separately from each of the two wire planes. Then a clustering algorithm which searches for a set of subsequent points ("clusters") among the hits found by the signal processing is carried out. In case of a straight muon track, a linear fit through the hits belonging to the "cluster" is performed separately on each view. This fit gives the parameters (slope and intercept) of each of the two 2D track projections. For each track one accomplishes a geometrical 3D reconstruction by employing an analytical approach: the "geometrical 3D track" is derived combining the parameters of the 2D track projections in order to obtain the track direction in space (zenith angle θ, azimuth angle ϕ) and the three coordinates (x_0, y_0, z_0) of a point belonging to the track.

The total sample of single muon events amounts to 1654 events (1247 triggered using the internal PMT system and 407 triggered by the external scintillators system). Applying quality cuts to both 2D views of the tracks (minimum track length, good χ^2 on the result of the linear fit) and the 3D reconstruction procedure, the statistics is reduced to 940 events (768 and 172, respectively, known hereafter as the "selected" events). Among the "selected" events triggered by the internal PMTs, 294 events show muon tracks crossing the whole drift length.

In Fig. 12 we show, as an example, the 3D geometrical reconstruction of a sample of single muon events recorded in one run (all superimposed in the same picture) triggered by the system of external scintillator planes. For these events the angular distributions reflect the geometry of the trigger set-up. For the majority of the events the observed zenith (θ) and azimuth (ϕ) angular ranges are $[45°, 70°]$ and $[260°, 280°]$, respectively. This is in agreement with expectations from the evaluation of the geometrical acceptance of the external trigger system.

The geometrical 3D reconstruction can also be applied to display the spatial topology for more

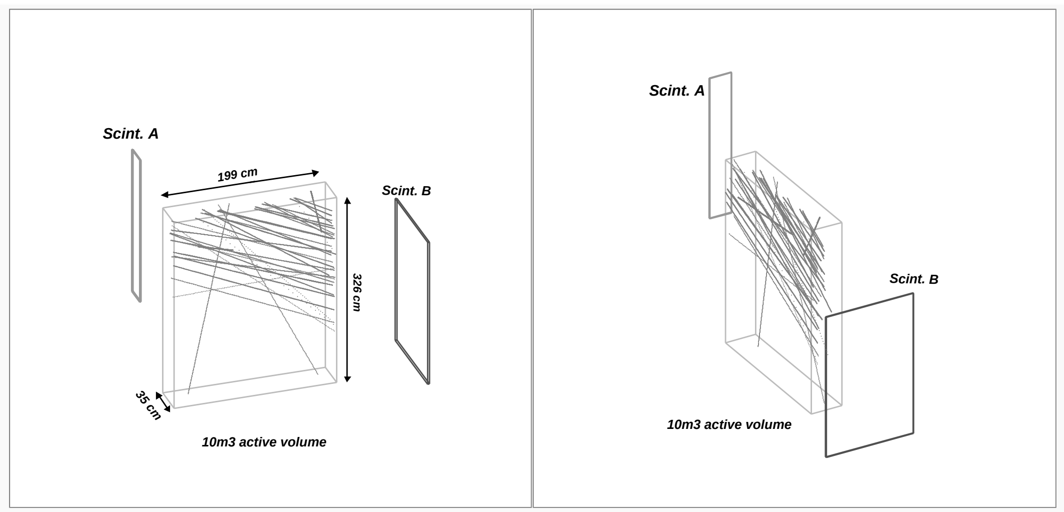

Fig. 12. 3D geometrical reconstruction: sample of superimposed muon tracks crossing the 10 m^3 active volume (viewed from two different angles). Each track is identified by a linear fit through the "cluster" of aligned hits provided by the signal processing algorithms. The trigger is provided by coincidence signal from the external system of scintillator planes (also shown). The sample of tracks shown here belongs to the "selected" muon sample.

complicated events. As an example, we report here, the reconstruction of a single event recorded with the 10 m^3 (Run # 641, evt. # 14). The two 2D view images are shown in Fig. 13 (top). An interaction vertex with several tracks propagating in the LAr sensitive volume is clearly visible. Five

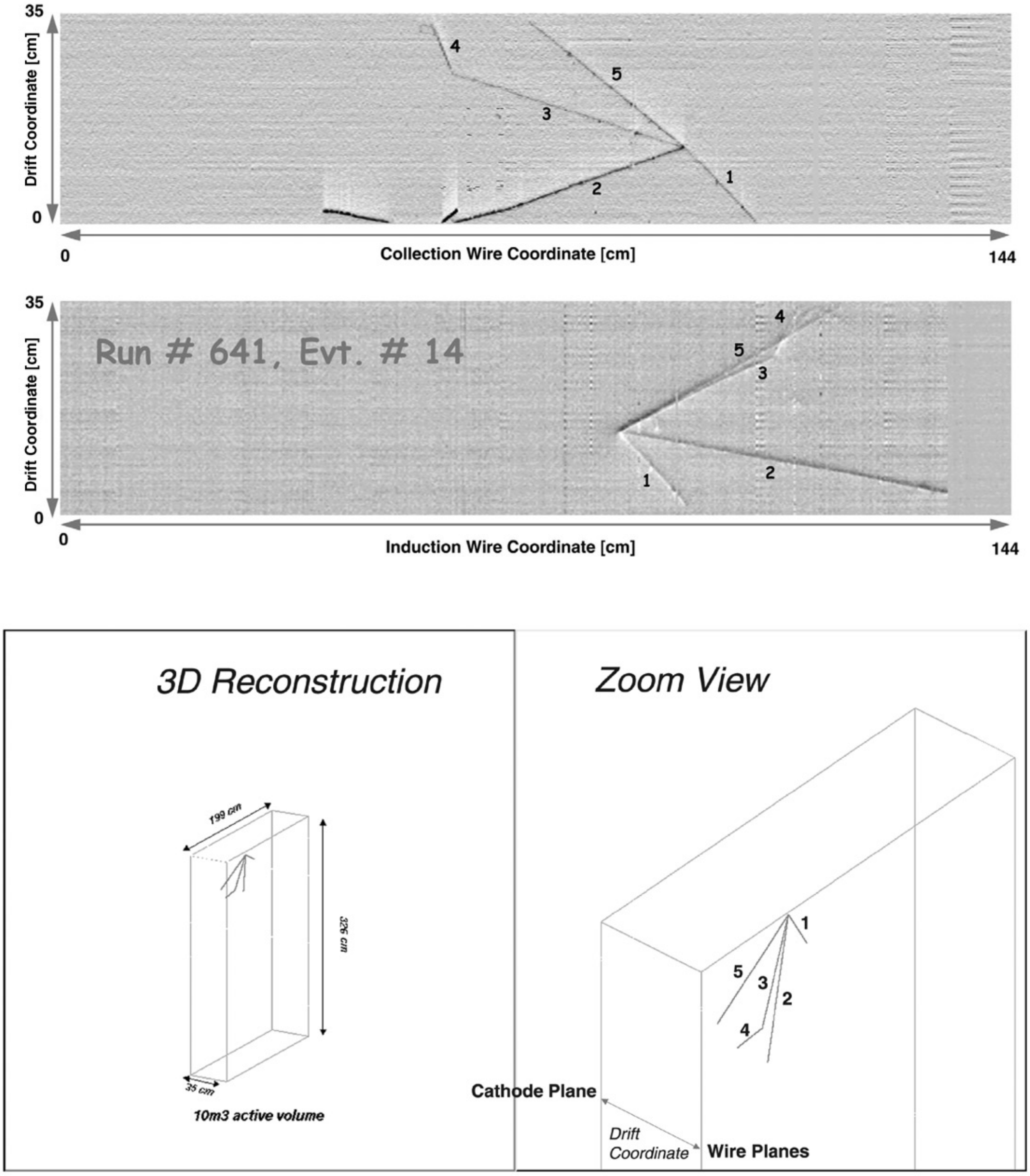

Fig. 13. (Top) 2D images (from the collection plane and from the induction plane) of an interaction event recorded during the 10 m^3 run (internal PMT trigger). (Bottom) Geometrical 3D reconstruction of the event. Five tracks can be associated to the vertex. The interaction is presumably due to a neutral particle entering the LAr active volume from above. Tracks # 1 and # 2 correspond to particles exiting the sensitive volume from the wire plane, Tracks # 4 and # 5 correspond to particles exiting from the cathode plane, while Track # 3 is fully contained in the LAr sensitive volume. Track # 4, showing δ-ray activity, is associated to Track # 3 (kink or decay).

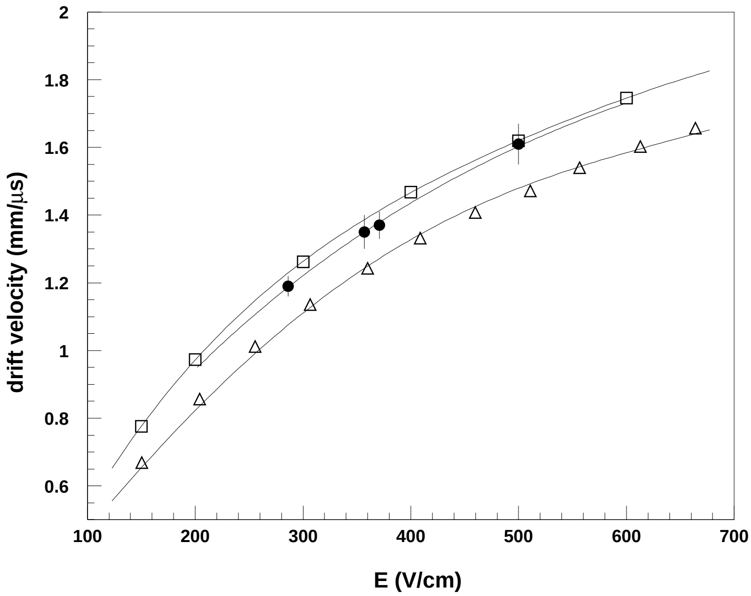

Fig. 14. Electron drift velocity in LAr as a function of the electric field, as measured in the 10 m^3 detector at $\sim$88 K (full dots). For comparison, measurements of drift velocity from the "3 t prototype" are also shown: open squares correspond to measurements at 87 K, open triangles to the ones at 92 K. Polynomial functions to fit the data are reported.

tracks associated with the vertex are visible on both views.[2] The 2D track projections on the two views have been one-to-one associated without ambiguities by superposition of the relative time windows. This provides the geometrical 3D reconstruction of the event shown in Fig. 13 (bottom). The topology of the event is compatible with an incoming neutral particle (presumably a neutron) entering the detector volume from above and undergoing a nuclear interaction with a multi-hadron system emitted in the final state.

7. Electron drift velocity

In order to measure the electron drift velocity in LAr we have used a sub-sample of the single muon events triggered by the internal PMT system (see Section 6). All the tracks in this sub-sample cross the whole drift region from the wire planes to the cathode or vice versa. Events have been individually selected by visual scanning and classified according to the different values of the electric field applied in the drift region. The drift path of the ionization charge along these tracks ranges from 0 to 35 cm (the sensitive volume thickness). For each track one calculates the time interval between the peak time of the waveform signals corresponding to the track points when crossing the anode and the cathode. The drift velocity is measured relating the time interval to the drift path. The mean value and relative error of the drift velocity from the track samples at different electric fields are reported in Fig. 14. On the same plot, for comparison, the measurements done with the ICARUS "3 t prototype" [11] in the same range of electric fields are also shown. The values corresponding to the "3 t prototype" (open squares) for a reported temperature of the medium of 87 K are close to the measurements with the 10 m^3 detector (full dots), for which the LAr temperature in the cryostat during operation was $\sim$88 K.

[2] Two additional track segments not associated to the vertex are visible in the *collection* view. These are not observed on the *induction* view, since they are outside the instrumented region in this view.

8. Calorimetric reconstruction

The 3D geometrical reconstruction described above is the first step of the procedure applied for a calorimetric measurement of the single muon event sample. Subsequently, determination of the energy release in LAr by ionizing events is performed by a number of further steps: (1) accounting for the charge loss due to attachment to electro-negative impurities (i.e. measurement of the electron life-time and of its behaviour during the run period) (2) charge to energy conversion with correction for the quenching effect in LAr.

8.1. Electron life-time

The analysis of the 10 m^3 events allows for an independent measurement of the drift electron life-time (τ_e) in LAr using the "selected" muons triggered by the internal PMT system (see Section 6). Estimates of τ_e are obtained directly from the attenuation of the signal amplitude observed at increasing drift distance from the wire chamber.

The hit amplitude measured on a wire (Q') represents the portion of ionization charge along the muon track detected by the wire. Data from the *collection* view have been used. To calculate the charge released per unit track length (dQ/dx), the "track pitch length" Δx (i.e. the effective length of the track "seen" by the wire) must be taken into account:

$$\frac{dQ}{dx} = \frac{Q'}{\Delta x} \quad \text{with} \quad \Delta x = \frac{\delta}{\cos(\gamma)} \tag{3}$$

where, as indicated in Fig. 15, $\delta = 0.3$ cm is the wire pitch and γ is the angle formed by the track direction and the direction of the *collection* wire pitch. The γ angle is a function of the zenith θ and azimuth ϕ angles of the muon track, obtained from the 3D reconstruction. The charge (expressed in number of electrons) is obtained by conversion of ADC counts (hit amplitude) with a suitable calibration factor coming from the test-pulse calibration of the electronic chain.

The distributions of dQ/dx have been computed grouping the hits according to their drift coordinate in 2.5 cm wide slices to account for the attenuation of the signal amplitude at increasing drift distance from the wire plane. As an example, in Fig. 16 we show a set of four distributions corresponding to the slice #1, #3, #5 and #7, out of the 14 slices in which the 35 cm drift distance is subdivided. The event sample is composed of data collected in few consecutive runs within a 24 h

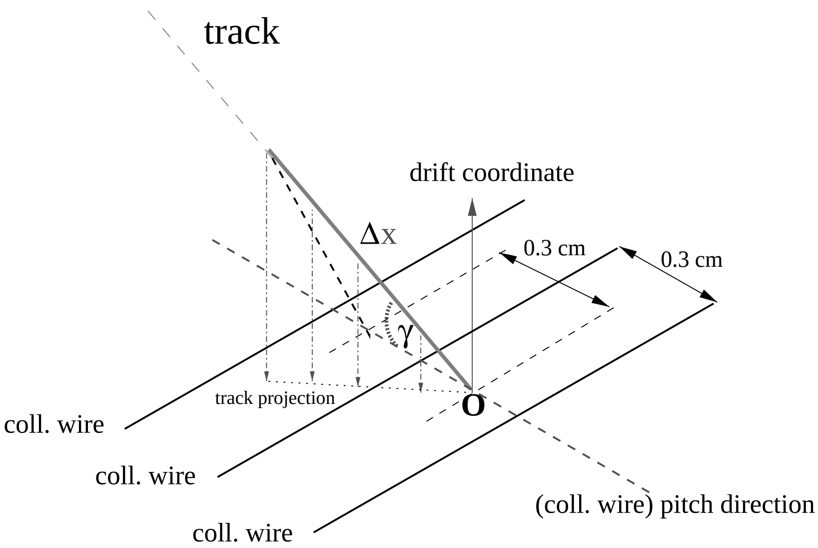

Fig. 15. Determination of the track pitch length Δx. A straight track crossing the collection plane is shown. The wire pitch is 0.3 cm. Definition of the γ angle between the track direction and the direction of the collection wire pitch is shown.

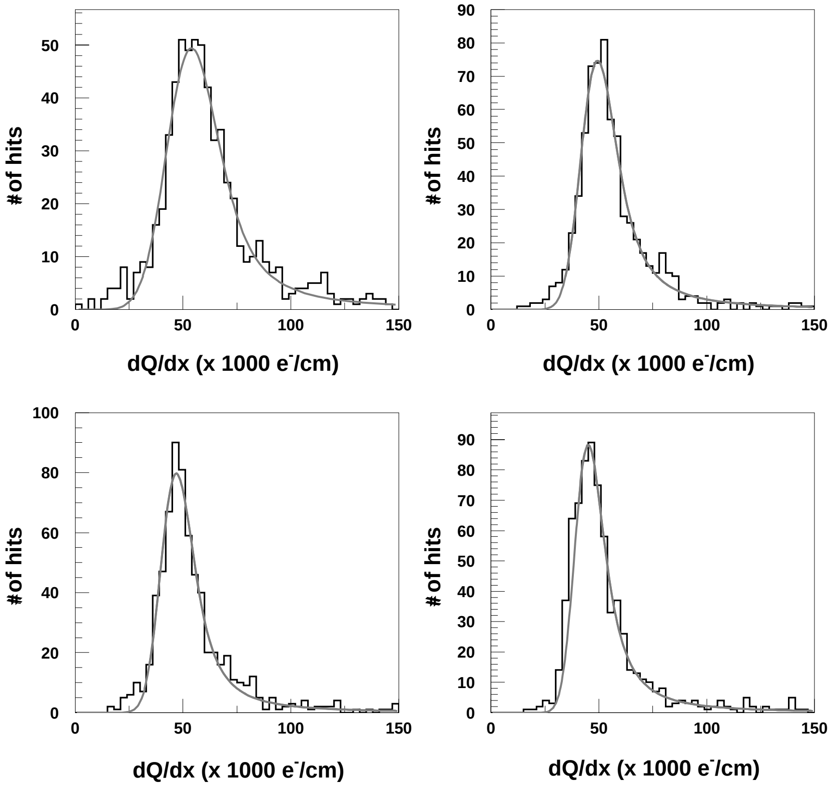

Fig. 16. Distributions of the charge per unit track length measured on the collection wires for a sample of single muon events. The distributions refer to four different slices of the drift coordinate ([0, 2.5] cm, [5, 7.5] cm, [10, 12.5] cm and [15, 17.5] cm, respectively). Each distribution is fitted with a convolution of a Landau function and a Gaussian function (continuous line).

"period" at 286 V/cm of electric field. Each muon track provides a number of hits (entries to the histograms) depending on the actual track length and direction with respect to the wire planes. The tracks selected for this analysis are those traversing the whole drift distance, i.e. contributing to each slice with about the same number of hits.

To measure the electron life-time in LAr, the value of the most probable charge per unit track length is first extracted by fitting each histogram with the convolution of a Landau function with a Gaussian function. The Landau distribution describes the fluctuations in the energy loss of a particle through matter due to the intrinsic statistical nature of the ionization process. The Gaussian function describes fluctuations in the measured charge due to various sources, the main one being electronic noise. Other contributions are due to the muon spectrum, to the track pitch length, to the effects of finite life-time and of electron diffusion. The fitted functions for the four drift slices of Fig. 16 are displayed. The average r.m.s. of the Gaussian from the fit in the various slices is 6500 electrons per cm. This corresponds to a contribution of about 1950 electrons to the spread of the single wire signal, mainly coming from electronic noise. This is in agreement with the design equivalent noise charge (ENC) from 1300 to 1800 electrons [13]. The ENC value is mainly due to the total capacitance at the input of the amplifiers (V791 Board, Section 5.2). The total input capacitance, sum of the wire and the cable capacitance, may vary according to the different length of the instrumented wires of the *collection* plane in the range from about 200 pF to about 500 pF.

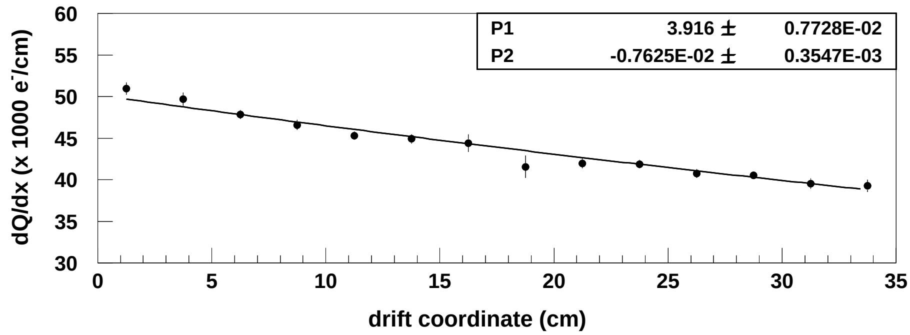

Fig. 17. Exponential fit of the most probable values from the 14 distributions of the charge per unit track length as a function of the drift distance (centre of the slice). Errors on the data points are from the individual fit in the corresponding slice and refer to statistical fluctuations. The parameter P_2 gives the inverse of the electron mean free path ($\lambda = -1/P_2 \simeq 131$ cm).

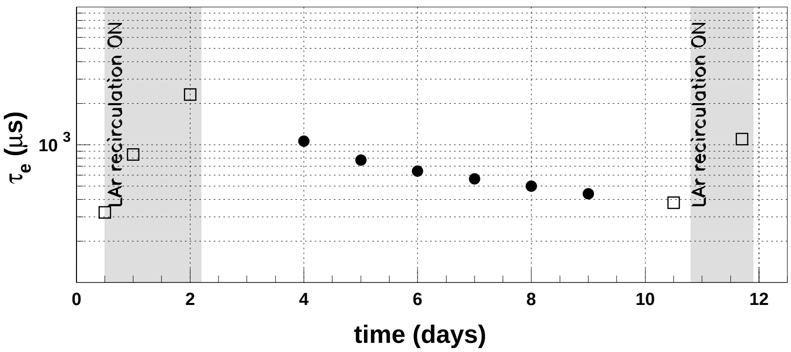

Fig. 18. Measurements of the electron life-time in LAr in a 12 days long period during the LNGS run: data from the analysis of the "selected" crossing muon sample (full dots) and values from the LAr purity monitors (open squares). During this period the LAr purification unit was on in the shaded intervals and the GAr purification system was off.

An exponential fit to the most probable values of charge per unit track length as a function of the drift coordinate (centre of the drift slice) gives the electron mean free path. In the example shown in Fig. 17 an electron mean free path of (131 ± 6) cm is obtained. For this sample the measured electron drift velocity is 1.18 mm/μs, therefore the resulting value of the electron life-time is $\tau_e = (1.11 \pm 0.05)$ ms.

In order to evaluate the evolution of the electron life-time during the 10 m^3 test, other groups of consecutive runs taken in periods of 24 h each have been analysed separately following the procedure described above. In Fig. 18 life-time measurements for six consecutive periods are reported (full dots). These results are in good agreement with the values obtained independently using the LAr purity monitors, also reported in the figure for comparison (open squares). The typical trend in the evolution of the LAr purity level (Figs. 3 and 6) when both GAr and LAr recirculation systems are off is confirmed.

8.2. $\mathrm{d}E/\mathrm{d}x$ measurement

The values of the electron life-time reported in Fig. 18 have been used to account for the charge attenuation occurring during the drift process and thus to reconstruct the distributions of the "corrected charge" released per unit track length along the muon track ($\mathrm{d}Q_{\mathrm{cor}}/\mathrm{d}x$):

$$\frac{\mathrm{d}Q_{\mathrm{cor}}}{\mathrm{d}x} = \frac{\mathrm{d}Q}{\mathrm{d}x} e^{t_d/\tau_e} \tag{4}$$

where t_d is the drift time associated to the hit, obtained from the peak time of the hit and the T_0 of the event. Then, full calorimetric reconstruction of the events has been accomplished accounting for the quenching effect on the ionization charge. A semi-empirical model similar to the one developed by Birks to account for light quenching in scintillator media [14] has been adopted to convert $\mathrm{d}Q_{\mathrm{cor}}/\mathrm{d}x$ into energy released per unit track length ($\mathrm{d}E/\mathrm{d}x$):

$$\frac{\mathrm{d}Q_{\mathrm{cor}}}{\mathrm{d}x} = A\frac{(\mathrm{d}E/\mathrm{d}x)}{1+K_{\mathrm{B}}(\mathrm{d}E/\mathrm{d}x)}. \quad (5)$$

The values of the parameters A and K_{B} used in Eq. (5) are from measurements performed with the "3 t prototype" [11] and with the 10 m^3 [4] using samples of muons stopping in the LAr imaging volume. The charge density measured along the stopping tracks, at given distances from the stopping point, is compared with the corresponding energy loss from simulated events. This provides a measurement of the quenching effect on the ionization charges at the given intensity of the electric field applied.

The $\mathrm{d}E/\mathrm{d}x$ distribution obtained with the "selected" muon sample is shown in Fig. 19. The average energy release is $\langle \mathrm{d}E/\mathrm{d}x\rangle = 2.49 \pm 0.14$ MeV/cm. The result of a fit with a convolution of a Landau and a Gaussian function is also shown in Fig. 19. The fit gives the most probable value of the energy loss $\mathrm{d}E/\mathrm{d}x_{\mathrm{m.p.}} = 1.82 \pm 0.10$ MeV/cm. The quoted errors include statistical and systematic contributions. The systematic uncertainty is due to the errors on the calibration factor, on the Birks parameters and on the lifetime.

These results have been compared with the outcome of a dedicated Montecarlo simulation. For this purpose single down-going atmospheric muon events crossing the 10 m^3 active volume have been generated according to appropriate energy and angular (zenith and azimuth angles) distributions. A sample of events has been selected as triggered by the internal PMT trigger system and passing the same cuts applied to the experimental data. The simulation indicates an average energy of about 5 GeV for this cosmic muon event sample. The Montecarlo average energy release and the most probable value are in good agreement with the reported results obtained from the experimental data analysis.

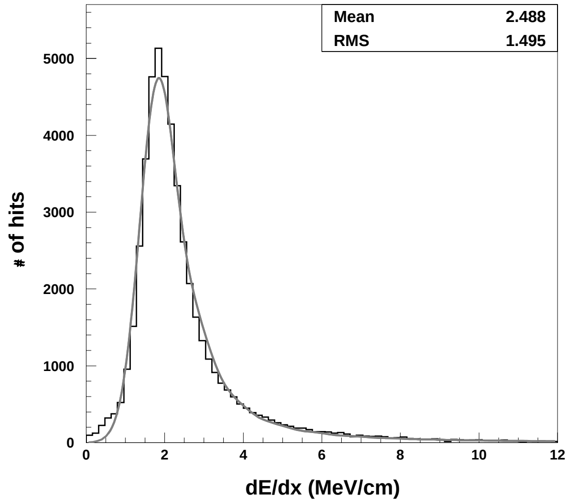

Fig. 19. Distribution of the energy per unit track length deposited by cosmic muons in LAr. Data refer to the whole "selected" muon sample. A Landau–Gaussian fit to the data is also reported (full line).

9. Conclusions

In this paper, we report on the long-term test of the 10 m^3 ICARUS LAr TPC prototype. The test measurements allowed to explore some aspects related to the performance of the technique, in view of the larger scale T600 module and of its cloning to a full detector for the Gran Sasso laboratory. The solutions adopted for the cryogenics plant (including the forced Ar recirculation in liquid phase) and the functionality of the high voltage system were fully investigated. A preliminary layout of the on-line event acquisition system has been probed and some off-line reconstruction algorithms have been improved also in view of the T600 data recording and analysis.

The analysis of the cosmic muon data sample yields values of the drift electron life-time in good agreement with the independent measurements obtained using LAr purity monitors. This confirms the reliability of the calorimetric reconstruction of the events and demonstrates that an accurate control on this parameter is ensured. A study of the electron life-time evolution with time and working conditions of the LAr recirculation system has been carried out as well. Calorimetric reconstruction of the energy release by cosmic muons independent of the event geometrical topology yields a result for the mean energy loss in LAr in agreement with expectations.

In conclusion, the successful test phase of the 10 m^3 prototype concluded the *R&D* programme of the Collaboration, opening the way for the test and subsequent operation of the full scale T600 module.

Acknowledgements

We would like to warmly thank the many technical collaborators that contributed to the construction of the detector and to its operation. We are indebted to the Pavia and LNGS mechanical and electronics Workshops for the excellent quality of their work. In particular we acknowledge the precious contribution of A. Capsoni, F. Vercellati and R. Nardó from the Pavia-INFN Mechanical and Electronics Workshops and of A. Candela, M. De Deo, M. D'Incecco and D. Corti from the LNGS and Padova-INFN Electronics Workshops. We also thank A. Donati and S. Parlati from the LNGS Computing and Network Office for the assistance during operation. The Gran Sasso Laboratory is kindly acknowledged for hosting the detector and contributing to the successful data taking. Finally, we are glad of the financial and technical support of our funding agencies and in particular of the Istituto Nazionale di Fisica Nucleare (INFN), of ETH Zürich and of the Fonds National Suisse de la Recherche Scientifique, Switzerland.

References

[1] P. Cennini, et al. (The ICARUS collaboration), A first 600 t ICARUS detector installed at Gran Sasso Laboratory, Addendum to ICARUS proposal, LNGS 95/10, 1995.
[2] F. Arneodo, et al. (The ICARUS collaboration), ICARUS T600, LNGS Annual Report 2001, LNGS/EXP-02/02, 2002, p. 113.
[3] F. Arneodo, et al. (The ICARUS collaboration), ICARUS: imaging cosmics and rare underground signals, LNGS Annual Report 1999, 2000, p. 87.
[4] E. Bernardini, Performance of the 10 m^3 Liquid Argon ICARUS module, Ph.D. Thesis, Università di L'Aquila, 2002, (available at the ICARUS Web site: http://www.aquila.infn.it/icarus).
[5] C. Rubbia, The liquid Argon Time Projection Chamber: a new concept for neutrino detector, CERN EP/77-8, 1977.
[6] F. Arneodo, et al., (The ICARUS collaboration), Detection of scintillation light in coincidence with ionizing tracks in a LAr TPC, Nucl. Instr. and Meth. A 432 (1999) 240.
[7] G. Carugno, et al., Electron Lifetime detector for liquid Argon, Nucl. Instr. and Meth. A 292 (1990) 580.
[8] F. Arneodo, (The ICARUS collaboration) Operation of a 10 m^3 ICARUS detector module, Proceedings of the Frontiers Detectors for Frontier Physics Conference, I.la d'Elba, Italy, 2000, Nucl. Instr. and Meth. A 461 (2001) 286.
[9] S. Centro, et al., Low-noise BiCMOS front-end and fast analogue multiplexer for ionization chamber, Nucl. Instr. and Meth. A 409 (1998) 300;
CAEN Technical Information Manual, 32 Channel ICARUS Analog Board, MOD. V791 (available at the CAEN Web site: http://www.caen.it).
[10] F. Arneodo, et al., (The ICARUS collaboration), Performance evaluation of a hit finding algorithm for the ICARUS detector, Nucl. Instr. and Meth. A 412 (1998) 440;
CAEN Technical Information Manual, 32 Channel ICARUS Digital Board, MOD. V789 (available at the CAEN Web site).
[11] P. Cennini, et al., (The ICARUS collaboration), Performance of a three-ton liquid argon time projection chamber, Nucl. Instr. and Meth. A 345 (1994) 230.
[12] E. Gatti, et al., IEEE Trans. Nucl. Sci, NS-26 1970 (2910).
[13] G. Franchi, A. Puccini, Measurements on the V791 board, CAEN Report 00100/98:V791x.rep0/00 (available at the CAEN Web site).
[14] J.B. Birks, Proc. Phys. Soc. A 64 (1951) 874.